Near Surface Geophysics, 2014, **12**, 493-504 doi:10.3997/1873-0604.2013059

First glacier-vibroseismic experiment – results from cold firn of Colle Gnifetti

Ulrich Polom[1,*], Coen Hofstede[2], Anja Diez[2,3] and Olaf Eisen[2,4]

[1] *Leibniz Institute for Applied Geophysics (LIAG), Stilleweg 2, D-30655 Hannover, Germany*
[2] *Alfred Wegener Institute Helmholz Centre for Polar and Marine Research (AWI), Am alten Hafen, D-27568 Bremerhaven, Germany*
[3] *Geophysical Institute (GPI), Karlsruhe Institute of Technology, Hertzstrasse 16, D-76187 Karlsruhe, Germany*
[4] *Institute of Environmental Physics (IUP), Heidelberg University, Im Neuenheimer Feld 229, D-69120 Heidelberg, Germany*

Received March 2012, revision accepted June 2013

ABSTRACT

In the summer of 2010, a small shallow reflection seismic experiment was carried out on the firn-covered cold glacier of Colle Gnifetti, Monte Rosa group, Swiss/Italian Alps. At this site, the physical properties of ice are comparable to polar conditions, which is why this site is often used for methodological tests. The experiment at 4500 m elevation was designed to explore the scope of shallow vibroseis for seismic targets within and below the glacier. A small ELVIS vibrator system was used to generate shear waves and compression waves for SH- and P-wave receiver setups of two profiles. The resulting sections clearly show a boundary from ice to rock around 60 m and deeper structures below the glacier. The deepest features are estimated to be 150 m for the SH-waves and 220 m for the P-waves. Reflections could be detected also within the ice overburden, which are preliminarily interpreted as a change of density in the upper 30 m and possibly crystal orientation fabric in the ice column. Furthermore, elastic parameters could be derived from seismic velocities, due to clear basement reflections. The results of this unique experiment enable new insights into the internal structure of ice masses and open a promising new investigation method for sub-ice structures and properties, such as basal sediments.

INTRODUCTION

Ice masses play a key role in the planet's global hydrological cycle, especially the global sea level. The internal structures and physical properties of ice masses represent an integrated memory, an image of their interaction with the environment. The behaviour of glaciers and polar ice sheets is receiving an increasing amount of attention e.g., for the prediction of dynamic ice movement and mass-balance processes. Most of the ice sheet dynamics of Antarctica or Greenland in regions of slow ice flow can be described by viscous internal ice deformation. Bed sliding or till deformation takes place in the more dynamic parts of ice sheets, such as ice streams and under temperate-based mountain glaciers. The movement of glacier ice masses is a direct interaction with the basement of the ice body, which varies from unfrozen, more or less water saturated sediment, to stiff rock. In the case of ice shelves and ice sheets the substrate ranges from water to a frozen bedrock and the range of interaction with the basement varies from water to a completely frozen base. The most dynamic parts of ice sheets are around the edges where the most rapid changes can take place. Ice movement here is largely determined by the interaction of the ice with the base. Ice can for instance move by sliding over hard bedrock, till deformation, deformation of the bed itself, or excessive deformation of a temperate ice layer (Cuffey and Paterson 2010).

In some cases the subsurface covered by an ice mass is the target of geophysical investigations, e.g., for locating a stratigraphic drilling target or for investigating geological settings or sub-glacial lakes and hydrologic systems in Antarctica. Therefore, active geophysical methods have already been widely used for ice and sub-ice investigations. Ground-penetrating radar (GPR) and radio-echo sounding are efficient tools to detect e.g., layers of included aerosol depositions from volcanic eruptions (Dowdeswell and Evans 2004), changes in crystal orientation fabric (Eisen *et al*. 2007) and the ice bed contact, because radar waves rarely penetrate into sub-ice formations. GPR techniques are ideally complemented by surface seismic methods, which, since the 1920s, are typically carried out by drilling and blasting of explosive charges in an adaptation land seismic exploration.

At first sight, the flat surfaces of cold glaciers' and ice sheets' accumulation areas (where the temperature is below the pressure melting point and the specific annual net mass balance is positive) seem inviting for active source seismics. However, a considerable problem occurs just below the surface. The upper tens of metres of such an ice mass are made up of highly porous firn,

* Ulrich.Polom@liag-hannover.de

which impairs the excitation of seismic waves (King *et al*. 1993; Sen *et al*. 1995; Benjumea and Teixido 2001). New deposition of snow on the surface results in a low density of the firn to nearly a third of the ice's density of 917 kg/m^3 (Cuffey and Paterson 2010). Over time the former surface layer is buried by additional accumulation and compacts. The pores in snow and firn are closed-off at densities >830 kg/m^3, usually reached at 30–120 m depth (the so-called firn-ice transition), depending on the location and environmental conditions.

Beneath the firn-ice transition, ice typically exhibits P-wave velocities of 3.8 km/s (Kohnen and Bentley 1973). Younger, more porous snow and firn formations above the firn-ice transition may vary in P-wave velocities from 0.5–3 km/s, depending on the interacting processes of snowfall, temperature, wind, percolating and refrozen meltwater, recrystallization and mechanical stress. Combined with the density gradient above the firn-ice transition, this velocity variation causes a continuous bend in the raypaths of the seismic waves and acts as a trap for seismic energy transmission.

This zone typically limits the plugging of blasting charges, which often requires drilling of boreholes more than 10 m deep, where stiffer parts of the formation are reached that prevent so-called 'blind shots'. Especially while using explosives, which are a common seismic source in the porous surface layer, a substantial fraction of the initial energy is lost by diving waves, inelastic deformation and the excitation of surface waves. This may require two charges, the first of which 'springs' the hole for the second. Nevertheless, only a small fraction of the initial energy transmits into the deeper parts of the formation as seismic body waves, as the far-field signal strength only increases with the cube root of the charge mass (Ziolkowski 1980).

Drilling for blasting charges is usually done by hot water, electromechanical or air-pressure techniques. It always involves a considerable amount of logistic support, time and energy. This effort is required since the quality of explosive charges is dependent on the depth of placement, to obtain sufficient elastic energy coupling. Furthermore, as the depth of such a seismic source is usually more than one wavelength below the surface, short-path multiples are commonly induced in the data recorded. Nevertheless, over the years, borehole explosive sources have been deemed the most effective compromise between production speed and data quality for seismic investigations on ice masses.
Many of the drawbacks associated with using explosives placed within firn can be overcome by using a surface based seismic vibrator (Eisen *et al*. 2010). The total seismic energy of a vibrator 'shot' is stretched over the time of a vibration signal (sweep), so instantaneous forces are much lower than using impulsive forces like explosives. This reduces the energy lost due to inelastic deformations, except for a small amount of firn compaction directly below the baseplate, which subsequently supports seismic energy transmission of subsequent sweeps. Further advantages of a vibrator source on firn are the increased productivity due to the absence of drilling operations, reduced costs, less diving wave generation and an excellent repeatability and control of the source signal. The latter especially supports the repeatability of experiments at a same source position e.g., for parameter testing, VSP operations and time-lapse seismic, which is a considerable disadvantage when using blasting charges in boreholes. In August 2008, the LIMPICS (Linking micro-physical properties to macro features in ice sheets with geophysical techniques) research group carried out an initial geophysical test survey at the field site Colle Gnifetti, Swiss Alps, using radar and shallow seismic investigation methods. The aim of the 2008 LIMPICS survey was the evaluation of joint radar and seismic methods for a detailed investigation of the firn and ice cover. For the seismic survey, the SISSY shotgun source was used (Diez 2013). The results showed limited success, probably caused by typical charge depths of only approximately 1 m. Thus, after successful application of a heavy 16 t vibrator source in Antarctica (Eisen *et al*. 2010), the seismic survey on Colle Gnifetti was repeated in August 2010 using the lightweight electrodynamic driven ELVIS vibrator source (Druivenga *et al*. 2011). The source was used to generate P- and SH-waves by vertically and horizontally shaking the vibration generator unit, recorded by vertical and horizontal geophone setups, separately. First of all, this enabled a comparison of the results from the different source types used in the 2008 and 2010 experiments. Also, the different wave types allow us to combine the results for the structural analysis and elastic parameter estimation presented in this paper.

SITE DESCRIPTION

Colle Gnifetti is a small glacier saddle at the top of the Monte Rosa group, (Swiss-Italian Alps) lying at 4450–4560 m a.s.l. (Fig. 1), forming the uppermost accumulation area of Grenzgletscher. The pass is covered by a nearly horizontal and surface parallel layered package of ice and firn several tens of metres thick.

Due to the climatic conditions, with temperatures mostly below the freezing point throughout the year and the topographic settings at this plateau-like location, the physical properties of the firn and ice are comparable to polar regions. Therefore, the location is widely used for palaeoclimatic investigations of the pre-industrial central European climate and testing of methods. Accommodation is conveniently available from the nearby mountain hut Capanna Regina Margherita, the highest-located hut in Europe, operated by Club Alpino Italiano. This setting enables a logistically convenient stay for extended experiments and a safe shelter in the case of a rapid change of weather conditions. Equipment transportation to the test site is only possible by helicopter cargo, which restricts the investigations to flight cargo adapted geophysical equipment of less than 400 kg per unit. A special challenge for the equipment and the crew are the environmental conditions of below-freezing temperatures, the reduced atmospheric pressure at this altitude and the often rapidly changing weather conditions. Therefore, to avoid altitude sickness at least two days of acclimatization are required prior to reaching the survey location.

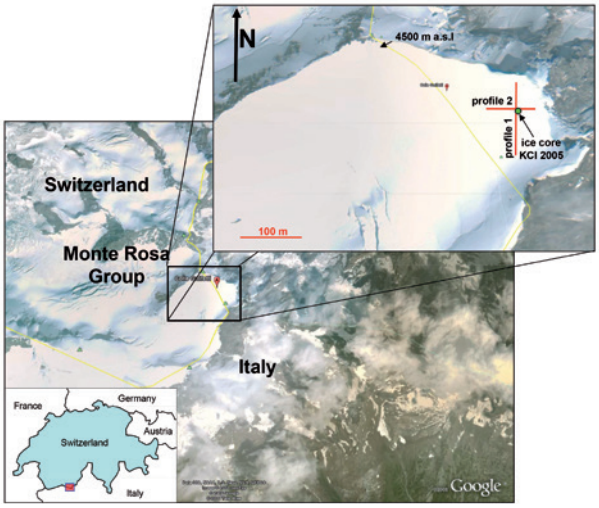

FIGURE 1
Location map of probably the highest-elevated (vibro-)seismic survey ever performed in Europe, nearly 4500 m a.s.l. at Colle Gnifetti, close to the Swiss-Italian border. On two cross-arranged profiles, shallow P- and S-wave reflection surveys were carried out during three days in August 2010 by the LIMPICS team to evaluate the capabilities of vibroseis sources on firn and ice and the prospects of P- and S-wave surveys for ice and sub-ice investigations. The location KCI (2005) refers to the position of the ice-core drilling in 2005, which detected first gravel units in the ice 62 m below the surface. The advection over five years is approximately 5 m. The location was close to the profile crossing. The red lines show the resulting CMP profiles, whereas source locations extend the lines up to 25 m (where possible) due to the offset vibration points (photos courtesy of Google Earth).

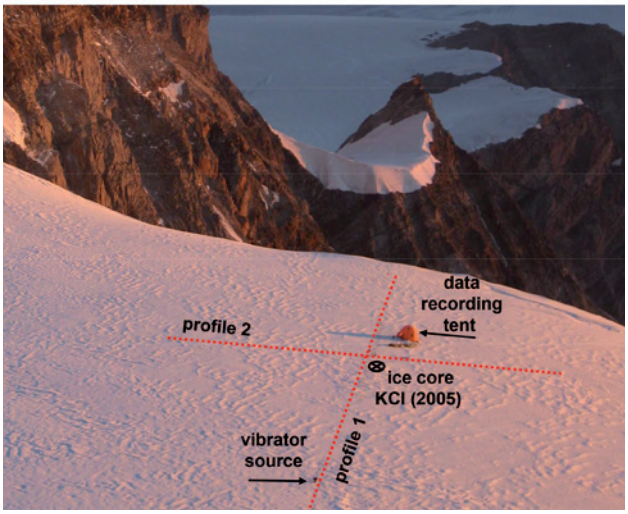

FIGURE 2
Impression of field setup (view from the Capanna Regina Margerita mountain hut). All equipment and crew transportation was carried out by helicopter by Air Zermatt. The orange tent was used for the recording operation (photo courtesy of A. Diez).

Colle Gnifetti constitutes a key site for long-term ice-core records from the Alps and has been investigated through several glaciological and ice-core drilling projects (Döscher *et al.* 1995), providing basic information on glaciological properties and dynamics. The mean surface mass balance is around 0.1–0.15 m water equivalent per year (e.g., Wagenbach 2001). Several radar studies have been carried out over the last decades, with varying equipment and targets, e.g., mapping ice thickness or connecting ice-core drill sites by isochronous ice-internal reflections (see Eisen *et al.* 2003, for a summary). In the area of investigation, the firn formation at the top is approximately 28 m, as evaluated by an ice core (referred to as KCI) drilled to a depth of 62 m below the surface in August 2005 (Bohleber 2008). Despite a mean annual air temperature of around –15° C (Haeberli and Alean 1985) and around –11° C at the ice-bedrock interface, occasional surface melting leads to the formation of some cm-thick melt layers, which intersperse the firn column as so-called ice lenses but also form continuous layers detectable by radar. The Monte Rosa rock mass below the glacier consists of gneiss and granite, strongly faulted during the uplift of the Alps and partly outcropping on the 2000 m high Monte Rosa East face.

METHOD

Data acquisition

S-wave profiling at each profile was carried out using 47 receiver channels connected to StrataView and GEODE (both GEOMETRICS Inc.) recording systems of 24 channels each. Channel 48 was connected to the pilot sweep signal and was used for on-site signal analysis, recording parameter evaluation and quality control during acquisition. The horizontal geophones (10 Hz natural frequency) were planted, with orientation perpendicular to the profiling direction (SH configuration) at the snow surface in intervals of 1.5 m (Fig. 3). The ELVIS horizontally vibratory source unit was also used in the SH configuration (Fig. 3 small photo), resulting in a so-called SH-SH source-receiver configuration using horizontally polarized S-waves with respect to the profiling plane (Pugin *et al.* 2004; Polom *et al.* 2010). This type of S-wave is less affected by wave conversions, as compared to the vertical polarized (SV) S-wave type (e.g., Garotta 2000). To enable a sufficient resulting CMP-coverage of nominal 24-fold, the source interval was also set to 1.5 m, using source positions between the receivers and additional offset source positions to approximately 50 m offset at both ends of the profiles. These offset extensions raised the CMP-coverage in the centre part of the profiles to 48-fold.

After initial sweep frequency range tests at each profile, sweep parameters were chosen to be a 60–360 Hz linear upsweep of 10 s duration at profile 1 and a frequency range of 30–240 Hz for profile 2. At each source location, two sweeps with alternating polarity were generated. Record lengths of 11 s and 12.2 s were used due to hardware and software requirements. A 1 ms sampling interval was used. The recorded data were stored uncorrelated without recording filters applied to enable detailed

noise editing during subsequent data processing. This was required due to other geophysical surveying activities in the nearby vicinity and some alpinist visitors at Colle Gnifetti, which partly produced man-made noise due to walking besides the seismic profiles.

Subsequent P-wave profiling was carried out using the 24 channels of the GEODE system only, connected to 23 vertical geophones (natural frequency 14 Hz) in 3 m intervals, using channel 24 for the pilot sweep. For vertical force generation, the vibration generator unit of the source system was changed to 90 degrees, vertical orientation. Source intervals were set to 3 m, arranged between the geophones and source locations were extended to in-line offsets of approximately 50 m where possible. This setup results to a nominal CMP-coverage of 12-fold, raised to 24-fold in the profile centres due to the offset vibration points. After initial test recordings at each profile, the sweep parameters were set to 30–240 Hz linear upsweep, 10 s duration, at profile 1 (20–160 Hz range at profile 2), using a total recording time of 10.5 s. Only one sweep at each location was applied and the recorded data were stored in the same manner as for the S-wave profiles. These decisions and the shortening of the acquisition period were necessitated by an upcoming change in weather conditions. An overview of the recording parameters applied for the experiment is given in Table 1. Sweep frequency ranges were chosen after some tests on site mainly with respect to the reduction of surface wave energy. Later frequency analyses of reflection events during data processing show that especially P-wave sweep frequencies could be shifted to considerably greater ranges.

RESULTS

Seismic data processing and depth imaging

The profile geometry is shown in Fig. 4. Coordinates are in metres and are relative to the centre coordinate (1000, 1000). Absolute coordinates were not acquired due to time constraints. The yellow lines in Fig. 4 show the resulting midpoint ranges of the reflection profiling, which are slightly differing for P- and SH-waves due to different offset ranges used. At KCI, the ice thickness derived from radar and borehole logging is estimated to be around 62 m. Since the coring was stopped as soon as silt was indicated in the ice, there is a depth uncertainty of approximately 1 m towards larger depth (Bohleber 2011).

Correlated source gathers from both P- and SH-wave configurations show strong direct and surface waves, which greatly obscure reflected arrivals (Fig. 5a,b). Fortunately, the differences in propagation velocity of the different wave types and the reproducibility of the vibrator source meant that most of the surface wave energy could be removed by f-k filtering (see e.g., Yilmaz 2001) of single records for P- and S-waves (Fig. 5c,d). Further data processing including a band-pass filter, amplitude scaling, top muting and a fine-tuned stacking velocity analysis resulted in detailed stacked time sections with clear reflections from the base of the ice mass. Also deeper reflections within the rock mass could be clearly imaged in both sections.

After time-domain processing, the time sections were depth converted using individually derived conversion velocities based on the stacking velocity analysis. A comparison revealed that the seismically determined bed depth was 6 m shallower than the bed determined using the borehole. In contrast, the depth con-

FIGURE 3
Main photo: geophone arrangement (horizontal and vertical units, profile 2, western part) above the cloud cover. Geophones were only fixed by simple planting into the snow at the surface. Small photo: ELVIS vibratory seismic source in horizontal mode (photos courtesy of A. Diez).

verted S-wave section of profile 1 fits the ice-core results. A similar depth deviation was observed for the P- and S-wave depth sections of profile 2.

TABLE 1
Data acquisition parameters.

SH-wave survey (1. & 2. day):	
Instrument:	Geometrics GEODE 24 channels & Geometrics STRATA VIEW 24 channels
Recording:	12 s (1 ms), 2 s listen time
Source:	ELVIS, horizontal mode unit
Sweep:	Profile 1: 60–360 Hz linear, 10 s, 200 ms taper Profile 2: 30–240 Hz linear, 10 s, 200 ms taper
Vert. Stack:	2, alternating polarity
Src. space:	1.5 m
Rec. type:	SM6 10 Hz
Rec. space:	1.5 m
CMP-fold:	48 (max.)
Prof. length:	118.5 m profile S1, 97.5 m profile S2
P-wave survey (2. & 3. day):	
Instrument:	Geometrics GEODE 24 channels
Recording:	12 s (1 ms), 2 s listen time
Source:	ELVIS, vertical mode unit
Sweep:	Profile 1: 30–240 Hz linear, 10 s, 200 ms taper Profile 2: 20–160 Hz linear, 10 s, 200 ms taper
Vert. Stack:	1
Src. space:	3 m
Rec. type:	SM6, unknown Hz
Rec. space:	3 m
CMP-fold:	24 (max.)
Prof. length:	128 m profile P1, 93 m profile P2

To enable a first consistent structural comparison with respect to the bedrock reflection events based on the existing data, a simple and fitting compromise was to adapt the P-wave sections to the drilling results by depth shifts of +6 m and +8 m respectively (Figs 6 and 7). The density function of the ice core KCI was included in the depth sections to demonstrate the strong variation of this parameter in the firn formation. For this application, the original density function (Diez 2010) counted in intervals of 1 cm was resampled to 0.5 m intervals using a sliding window mean value calculation to adapt to the scale of the seismic section and for further use in the elastic parameter analysis. Furthermore, the density function was used to calculate the P-wave interval velocity by the density-velocity relationship for firn and ice published by Kohnen (1972) and its RMS equivalent. These density-derived velocity functions were compared with the seismically derived, borehole depth adjusted interval and RMS velocities at the ice core location in Fig. 8.

The density-velocity relationship at 61.5 m results in a RMS velocity of 3.282 km/s, which would shift the bedrock event from 39 ms two-way time (TWT) to 64 m in the depth domain, i.e., 2.5 m deeper than the borehole estimate. The borehole adapted seismic RMS velocity to fit 61.5 m is 3.158 km/s, the seismically derived RMS velocity was 2.846 km/s for profile 1. A strong RMS function misfit exists within 0–20 m, due to the lack of horizontal and vertical resolution in this depth range. The deviation in velocities from surface seismic analysis estimates needed further investigations. Assuming a P-wave RMS velocity of 3000 m/s for the bedrock event, the deviation of –6 m (–8 m) is equivalent to –4 ms (–5.3 ms) two-way timing error. Subsequent timing checks of raw data achieved no indications of a systematic timing error, e.g., due to trigger timing problems. Furthermore,

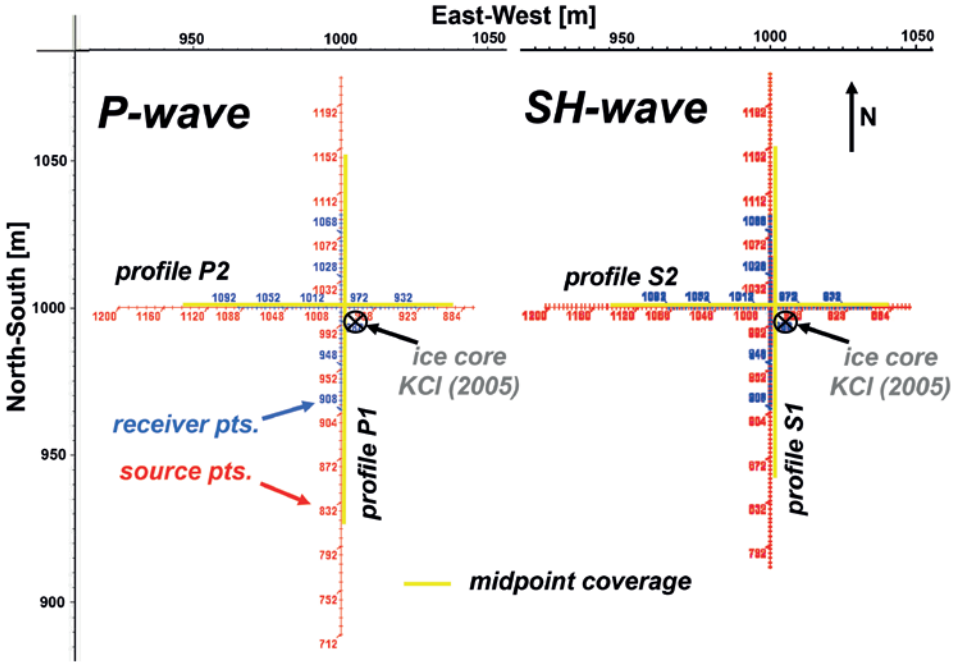

FIGURE 4
Resulting geometry setup of vertical (P-wave) and horizontal (SH-wave) sources (red lines and labels) and receiver (blue lines and labels) configuration (see text for individual spacing). Yellow lines indicate the covered midpoint ranges. Due to different offset source point ranges, the resulting midpoint ranges of P- and SH-waves are slightly different on profile 1.

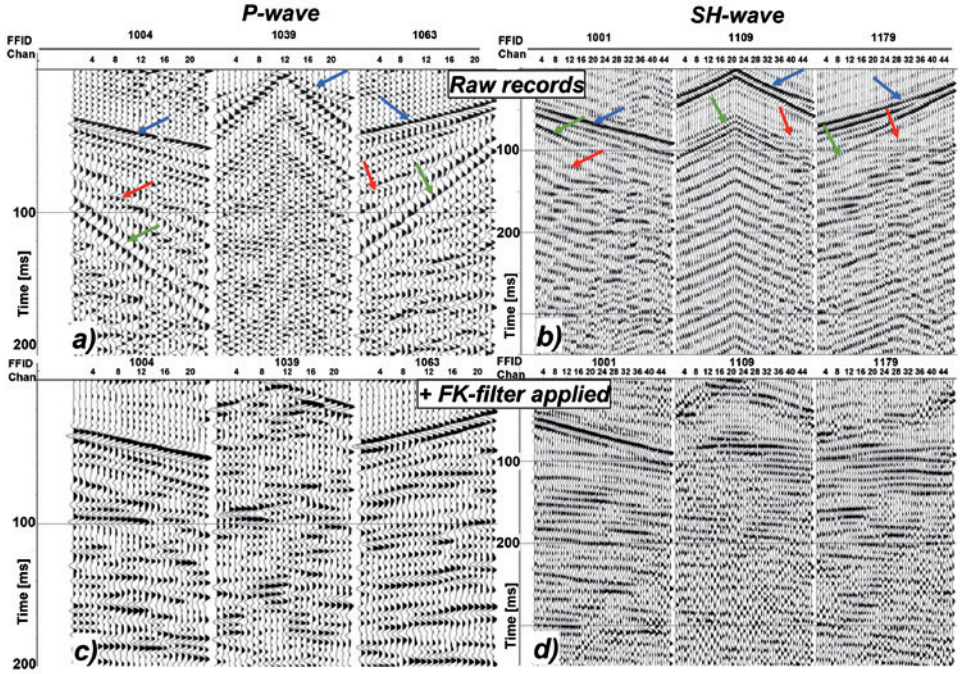

FIGURE 5
Correlated record examples of a) P-wave and b) S-wave setups from profile 1 with AGC scaling applied. Arrows indicate: red: reflection events; blue: direct waves; green: surface waves of a) Rayleigh-type and b) Love-type. c) and d) show the same records after f-k filtering to remove the surface wave content.

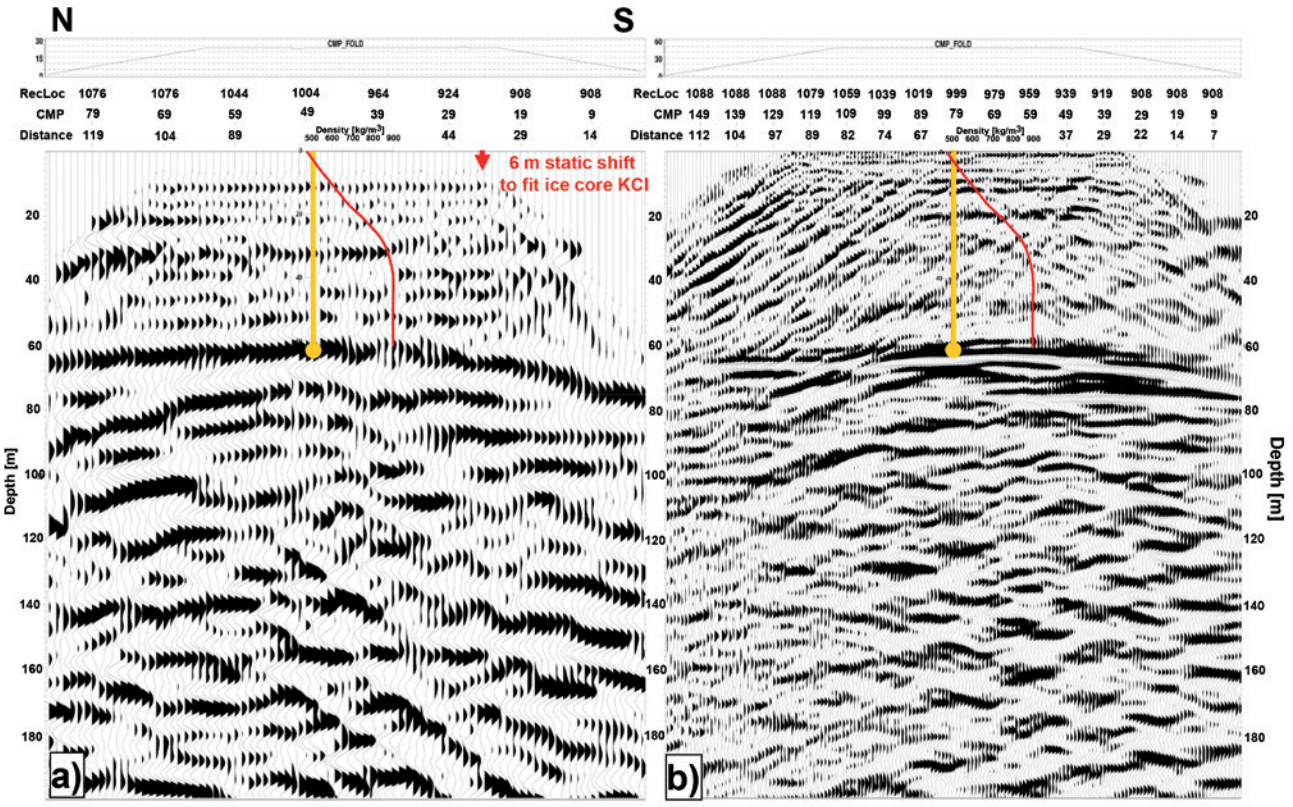

FIGURE 6
Depth converted stack sections of profile 1 a) P-wave and b) S-wave. The yellow mark indicates the profile crossing, where the base of the ice mass was encountered at 62 m below the surface during ice coring. The depth conversion of each wave type section was carried out independently by conversion velocities derived from stacking velocity analysis. After conversion, the P-wave section was shifted 6 m downward to enable a fit of the base reflector as the starting point for reflector correlation.

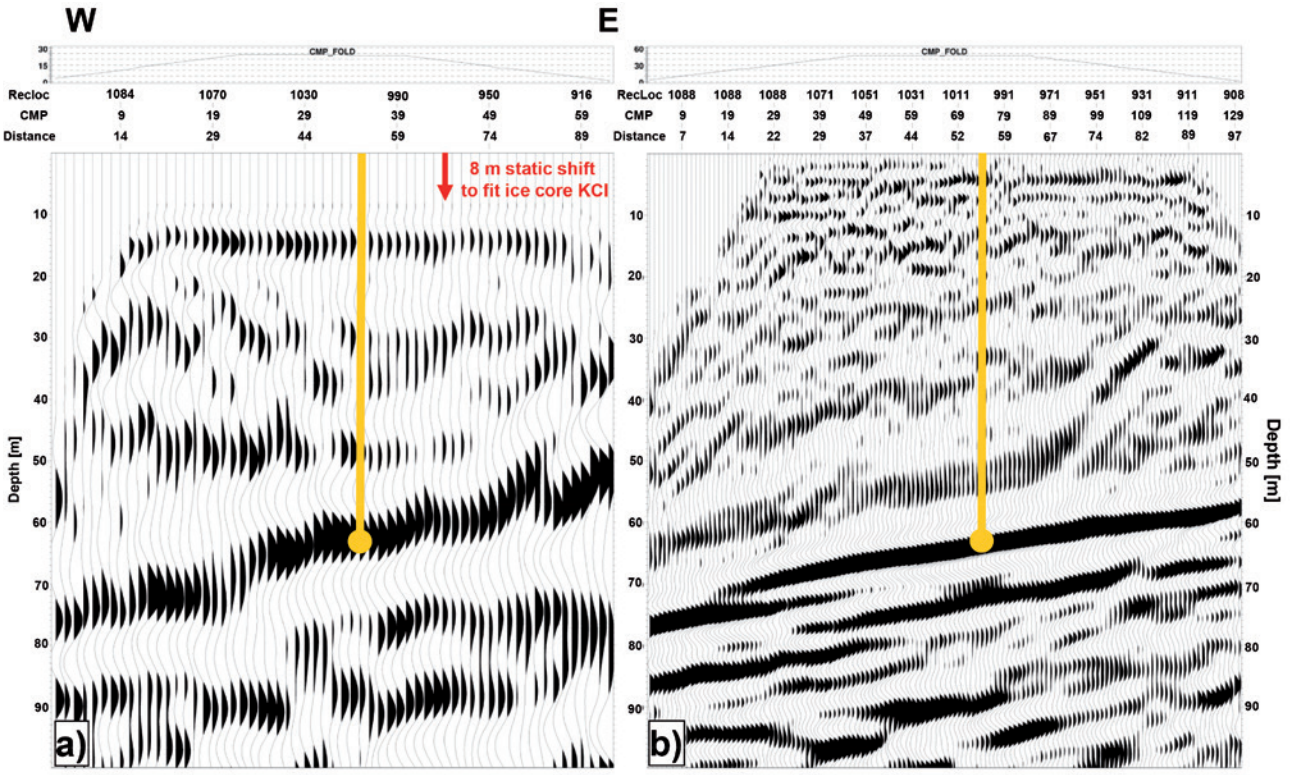

FIGURE 7

Depth converted stack sections of profile 2 for a) P-wave and b) S-wave, restricted to 100 m depth. As in Fig. 7, the yellow mark indicates the profile crossing and the depth of ice core KCI. After depth conversion, the P-wave section was shifted 8 m downward to enable a fit of the base reflector as the starting point for reflector correlation.

except for the geophones, the same recording equipment, nearly the same source system and the same vibroseis procedure were used for the P- and P-wave sections. Using the vibroseis method by recording the pilot sweep in each record as performed here includes an automatic trigger timing compensation during the vibroseis correlation process. Therefore, the estimated timing error was around 31 microseconds (1/32 of 1 ms sampling interval) following the technical specifications of the equipment used.

Other possible causes of the timing error include: 1) a significant change of the wavelet from the expected zero phase characteristic to earlier times due to snow compaction during the vertical operating vibrator sequence, or 2) errors in the P-wave velocity field introduced by errors in the hyperbolic moveout analysis used for determining the velocity model. Cause 1) could not be verified since only one record was acquired at each location of profiles 1, and 2) was expected to be less than the sampling interval.

Cause 2 is thought to be feasible since the basement reflector hyperbola images of the CMP common offset gathers were more coherent for S-waves than for the P-waves, even due to the double CMP coverage. This resulted in equivalent CMP stacking results for different hyperbola interpretations for the P-wave profiles in the range of the excepted error. Furthermore, non-linear raypaths due to the strong gradient in the firn and probably horizontal-to-vertical anisotropy could also not be excluded as the cause of the misfit. Such effects would probably lead to an extension of the calculated two-way traveltime for the offset traces and therefore result in slower RMS velocities. Etris *et al*. (2001) reported that a 10–15% depth error range due to such effects is not exceptional for P-wave reflection seismic without other *a priori* knowledge or data. We conclude that the cause of the misfit between the seismic derived depth section and the borehole estimate cannot be uniquely determined by this data set. Additional field experiments like Vertical Seismic Profiling (VSP) and P-wave profiles using higher CMP coverage are required.

The general data processing sequence applied for both profiles is shown in Table 2, including the velocity field processing shown in the later parts of this paper. The resulting depth sections after post-stack Finite Difference (FD) time migration (see e.g., Yilmaz 2001) applied using smoothed velocity fields derived from stacking velocities are presented as fence diagrams in Fig. 9(a) (P-wave) and Fig. 9(b) (S-wave). The grid sections show a good structure and phase agreement at the bedrock reflection and deeper events. The results for profile 2 differ slightly in the firn and ice region above, compared to profile 1, which is a consequence of the different frequency ranges used.

To check further depth uncertainties and to compare the scales of resolution, a comparison of the seismic results with the GPR results (Konrad *et al.* 2013) acquired in 2008 at the same

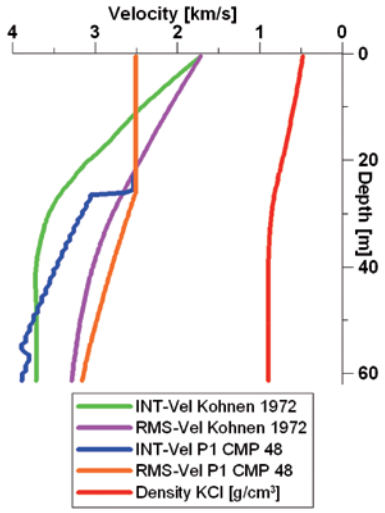

FIGURE 8

Seismic derived and depth adapted P-wave interval (blue) and RMS (orange) velocities from the centre of profile 1 compared to P-wave interval (green) and RMS (magenta) velocities derived from the density-depth function (red) of the ice core KCI using the firn and ice relationship published by Kohnen (1972). In the expected firn range 0–25 m there is a strong mismatch due to poor P-wave data resolution, below the different velocity functions approach in the depth.

profile was carried out. For this purpose, a cut of the GPR time section was adjusted to the position of seismic profile 1 and linearly scaled vertically to fit the depth of the ice core KCI. With respect to the limited penetration of the GPR section into the bedrock, the comparison was restricted to 80 m in depth. The resulting arrangement is shown in Fig. 10.

Considering the principle differences of the imaging capabilities of GPR and seismic methods due to the different physical parameters involved in both methods, this figure highlights the synergy of both methods with respect to the firn and ice regimes. For the firn regime, down to nearly 30 m in depth, the 250 MHz GPR achieves a resolution an order of magnitude greater than the seismic profiles. In the 0–30 m depth range, some similarities exist between the GPR and S-wave sections. In the ice depth range 30–62 m, the GPR section shows no reflections, whereas the P- and S-wave sections show partly comparable reflection patterns. For sub-bedrock imaging, the S-wave sections show the most detailed results, whereas GPR and P-wave sections show less clear bedrock topography.

Further verification and improvement of the seismic depth conversion velocities with respect to subsequent elastic parameter calculations required a fine tuning of seismic structure results and velocity data. This can be carried out by e.g., including cross checks with results from other laboratory ice core analyses, the GPR depth section and advantageously, from VSP. But, the arrangement and acquisition of the experiment was carried out as a principle test only. Therefore, the important additional data from e.g., VSP were not acquired and other depth evaluation data were not available. Thus fine tuning could not be carried out in a sufficient manner, because unevaluated assumptions need to be included. Especially, proofed specifications of the true depth of the rock surface were missing, which was neither reached by ice core drilling KCI nor available from the GPR section in sufficient accuracy (i.e., less than 2 m). A special problem is that the ice-bed transition in the GPR section is fuzzy. This is interpreted as a result of an increasing dirt content in the basal ice layers, which affects the propagation velocity and increases wave scattering.

DERIVATION OF ELASTIC PARAMETERS

Further processing was undertaken prior to elastic parameter estimation. This processing included basic tuning applied to the seismic sections shown in Figs 7 and 8 to fit the ice basement depth derived from the KCI maximum depth. The aim was to check the results of the elastic parameter calculation principally with respect to the inexactness included from probable errors in depth conversion and depth fitting. Elastic parameter calculations were restricted to the data of profile 1 to avoid additional uncertainties e.g., due to the different sweep frequency ranges used on profile 2, which resulted in lower resolution compared to profile 1 (Fig. 9a,b). In Fig. 9(a), well aligned main reflectors image dipping of the interfaces. Pattern differences in profiles 1 and 2 above the ice base were ascribed to the different frequency ranges used. Compared to the P-wave result, the imaging in Fig. 9(b) shows better resolution, especially below the ice base.

Interval velocities were calculated from the RMS stacking velocities using the Dix equation (Dix 1955) after application of a two-dimensional gradient smoother. Subsequently, the same depth fitting of the basement reflector applied to the P-wave depth section (Fig. 7) was applied to the P-wave interval velocity-depth function using a linear depth stretch. Interval velocity fields from

TABLE 2

General data processing sequence applied for both profiles. The parameters of processing modules applied were derived individually for P- and S-waves and for the individual profiles.

Data processing (P&S):
1. Corrupted record/trace detection and elimination
2. Record combination (S), geometry setup
3. Bandpass filter analysis
4. Amplitude scaling, bandpass filter, top muting
5. Fk-analysis, Fk-filter
6. Interactive velocity analysis, NMO correction
7. CMP-stacking, trace normalization (no statics – no elevation function available)
8. Reflection time checks using inlines and crosslines
9. FD-migration | FX-deconvolution
10. Depth conversion using smoothed stacking velocities
11. Depth check and adjustment (relative to ice core KCI)
12. Velocity field processing to calculate Poisson ratio, shear modulus, and using the density function from ice core KCI

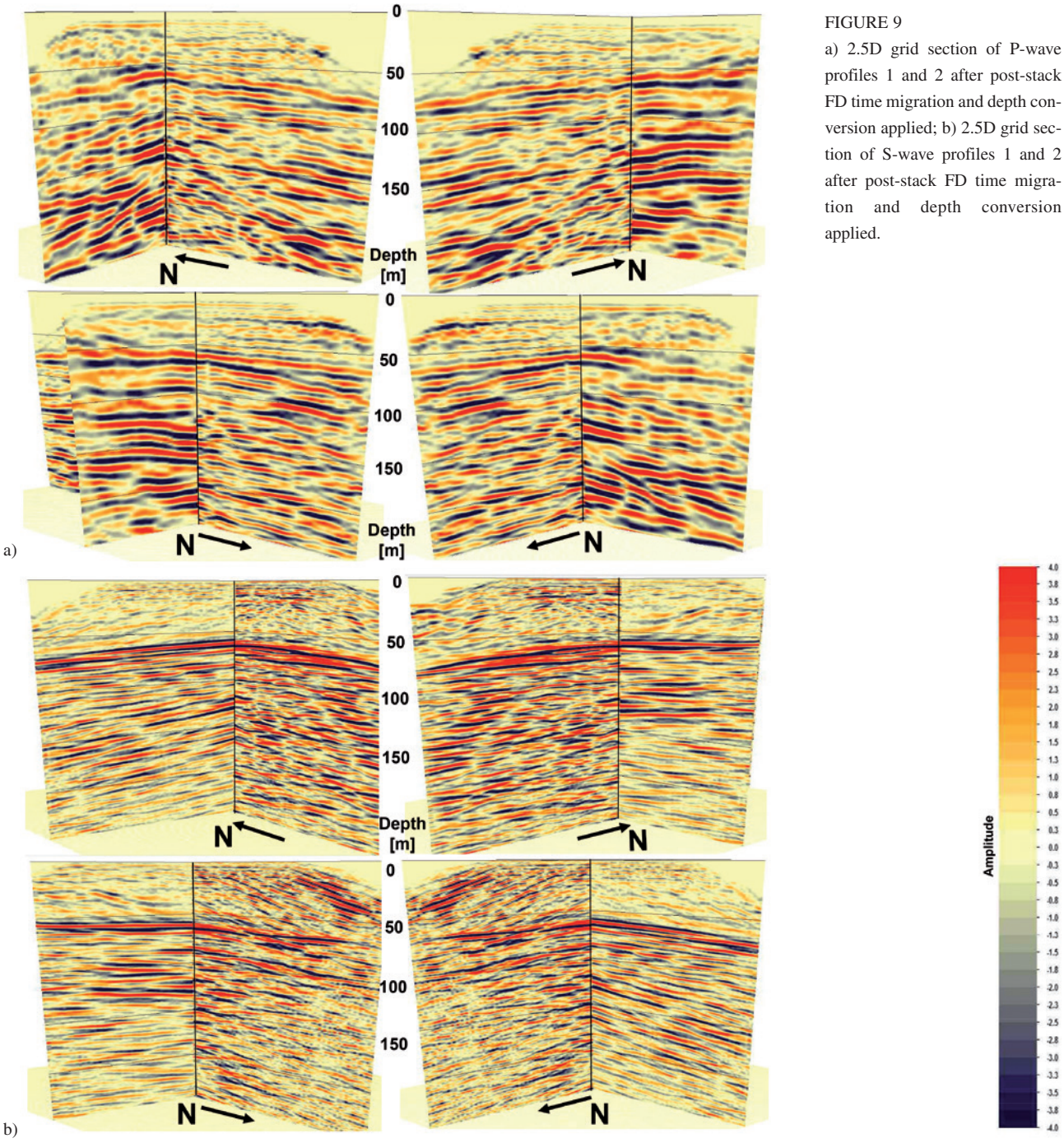

FIGURE 9
a) 2.5D grid section of P-wave profiles 1 and 2 after post-stack FD time migration and depth conversion applied; b) 2.5D grid section of S-wave profiles 1 and 2 after post-stack FD time migration and depth conversion applied.

P- and S-waves were then combined to calculate the Poisson ratio (Fig. 11). The calculation of the Poisson ratio was restricted to the overlapping area of P- and S-wave sections based on reflection seismic velocity analysis including depth adjustments applied. Since the Poisson ratio is not depending on density, the calculation is not depth restricted by the density function like the bulk modulus (K) or the shear modulus (G). Due to the inclusion of areas of poor P-wave velocity analysis possibilities, like the uppermost 20 m and in the bedrock below 61.5 m, the interpretation is restricted to the depth range 20–61.5 m. This range is dominated by low values and a slight lateral variation. A comparison with the Poisson ratio values published by King and Jarvis (2007) for a firn and ice column on Adelaide Island (included as a colour bar in the P-wave section in Fig.11 combined with the dotted density function) shows higher values in the range 20–40 m and similar values below 40 m.

The bulk and shear moduli were then calculated by combining the density function from the KCl ice core with the Poisson ratio

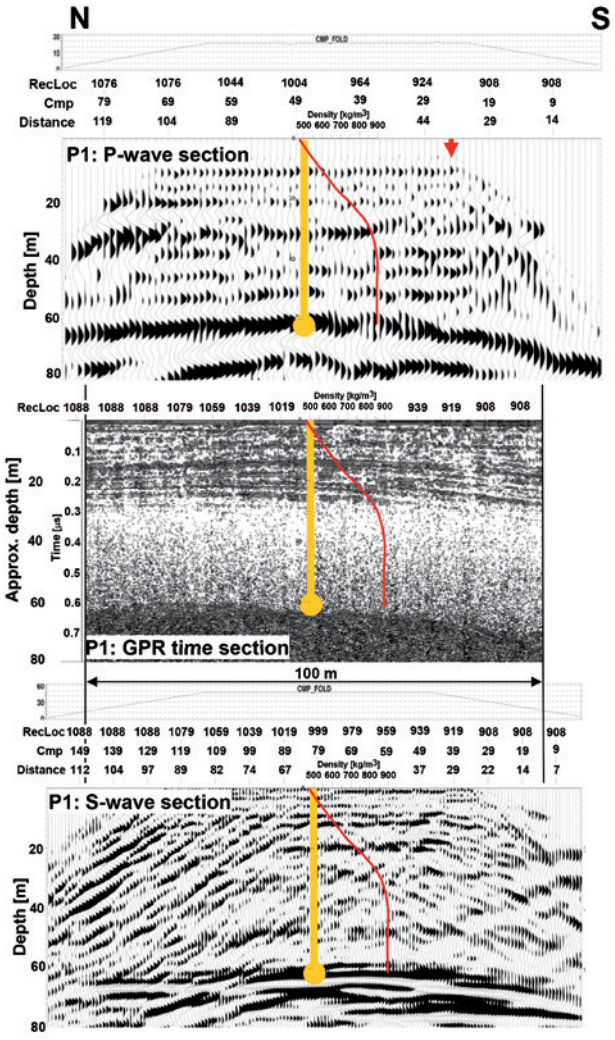

FIGURE 10

Comparison of depth converted P- and S-wave stack sections of profile 1 to GPR time section acquired in 2008 (Bohleber 2011). Depth adjustment was carried out to the maximum depth of KCI borehole only.

estimates obtained from the P- and S-wave velocity fields. The resulting parameter fields combined with seismic depth sections are shown in Figs 12 and 13, respectively. Due to the depth restriction of the density function these figures can only be interpreted to 61.5 m in depth. Whereas Fig. 11 shows a lateral variation of the G modulus in the depth 20–60 m, the lateral variation of the K modulus is smaller and more dominated by the increasing density function. Both parameters correlate to the expected ice depth range of 30–61.5 m.

DISCUSSION

Results achieved from this unique experiment originally designed as a small experimental feasibility study led to new insights from combined P- and S-wave reflection seismic surveying targeting glaciers and ice. The principle capabilities of P-wave vibratory reflection seismic surveying on firn and ice covers have already been pointed out by Eisen *et al*. 2010 using a 16 t exploration vibrator of 120 kN peak force, with a detailed analysis by Hofstede *et al.* (2013). We demonstrated that such investigations can also be carried out for shallow targets using only a 110 kg (low force) vibratory source of 0.5 kN peak force. This force is more than two orders of magnitude less than that of an exploration vibrator. The results achieved for P-waves also highlighted new capabilities for the successful application of a high-frequency bandwidth above the common frequency range of hydrocarbon exploration seismics for such targets. For the P-wave sections, common velocity analysis led to a mismatch of 10–15% at the estimated ice base compared to the borehole results, whereas S-wave velocities match. Also the resolution of the P-wave data is poor in the firn part from 0-30 m compared to the S-waves due to half of the CMP coverage and the non-sufficient geophone spacing for this depth range.

The S-wave results were the most unexpected for such an application environment. Because of the low density and low compaction conditions of the snow cover, the propagation of S-waves through this zone was unexpected. It was expected that strong absorption would affect especially the high-frequency part of the emitted signals. No special preparation of the vibrator baseplate and the source locations were carried out to improve the source-to-ground coupling, the source was used in the same way as in an operation on soil. The experiment showed that the high-frequency part of the emitted signals of 60–360 Hz could be used successfully for a clear image of the basement of the firn and ice mass at nearly 62 m depth, in contrast to the expected strong absorption of these frequency parts in the source spectra. Also, deeper parts within the rock below were imaged. No adaption of the derived S-wave velocity field was required during depth conversion to fit to the maximum depth of the ice core KCI, which was indicated as the base of the firn and ice cover.

Both P-wave sections showed misfits to the maximum depth of the ice core KCI after depth conversion. The misfit occurs for both P-wave sections with the same sign and similar magnitude, enabling us to apply the same correction at the crosspoint of the profiles. The most probable reason for this obviously systematic misfit is caused by a depth conversion velocity field error. We deem timing problems unlikely. The misfit most likely results from errors in the velocity field due to more misaligned reflection hyperbola figures in the P-wave data compared to the S-wave. One possible cause is anisotropy but this could not be clarified by the data of this first experiment alone and additional investigation is required. A comparison with a calculated velocity using the density-velocity relationship for firn and ice after Kohnen (1972) in Fig. 8 could also not clarify the depth mismatch. It shows similar RMS velocity functions in the depth range 25–61 m but the density derived velocities are higher than the borehole adapted velocities. Therefore an error range of at least 10–15% must be assumed due to this misfit for the subsequent calculations to derive elastic parameters from the velocity results. This uncertainty is similar to those encountered when determining ice thickness and bedrock topogra-

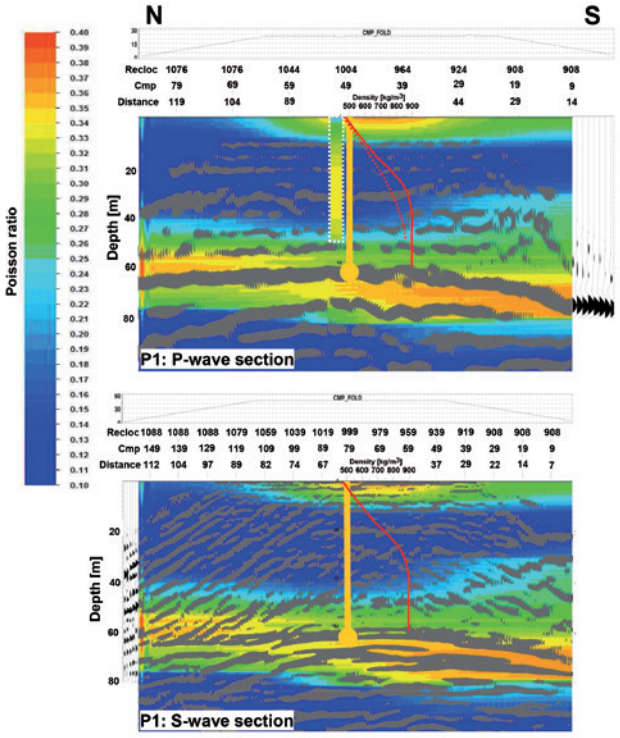

FIGURE 11

P- and S-wave depth sections (shaded) of profile 1 combined with a colour coded Poisson ratio field in the background. The Poisson ratio was calculated based on reflection seismic velocity analysis including depth adjustments to 61.5 m. For comparison, the Poisson ratio results published by King and Jarvis (2007) for a location on Adelaide Island in Antarctica are included as a colour bar in the P-wave section. The dotted red curve represents the density-depth function of this location.

phy for glaciers with GPR data (Moran *et al.* 2000).

Compared to the Poisson ratio results published by e.g., King and Jarvis (2007) for firn at Adelaide Island, Antarctica, the resulting range for the firn part is similar. King and Jarvis (2007) reported a maximum value of 0.34 in 31.5 m and a minimum of approximately 0.2 at the surface. However, in comparison to the variation of Poisson ratio published by King and Jarvis (2007), the resulting variation in depth for the Colle Gnifetti data is different in behaviour, since its depth function tends in the opposite direction. The reason for this discrepancy is as yet unknown and needs further investigations due to a lack of data for calibration and comparison. The G modulus values in the ice depth range are at maximum close to the values published by Gammon *et al.* (1983), who reported a G modulus of 3.521 GPa for polycrystalline ice from lab investigations. The calculated results for the K modulus are at maximum also close to the value of 8.899 GPa for polycrystalline ice (Gammon *et al.* 1983). So, these calculations fit in the expected range. A more detailed evaluation of the calculated elastic parameters and their vertical and lateral variation require additional investigations at Colle Gnifetti, or additional seismic experiments at well-known locations.

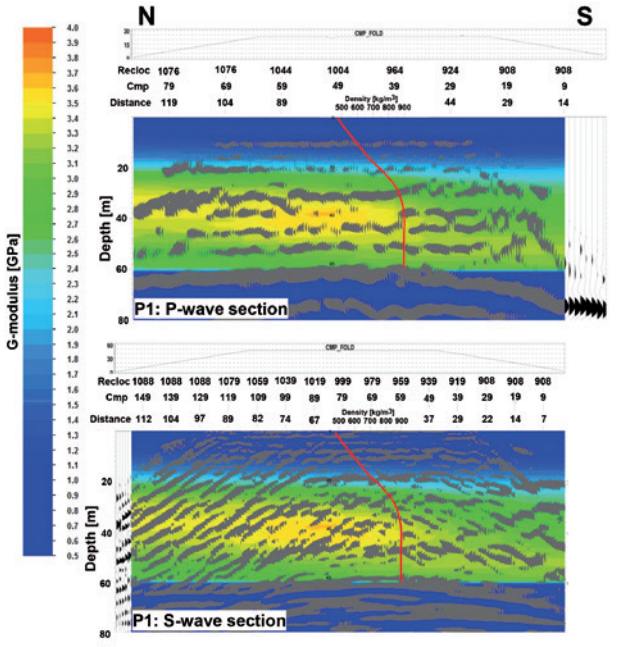

FIGURE 12

P- and S-wave depth sections (shaded) of profile 1 combined with a colour coded shear modulus field in the background.

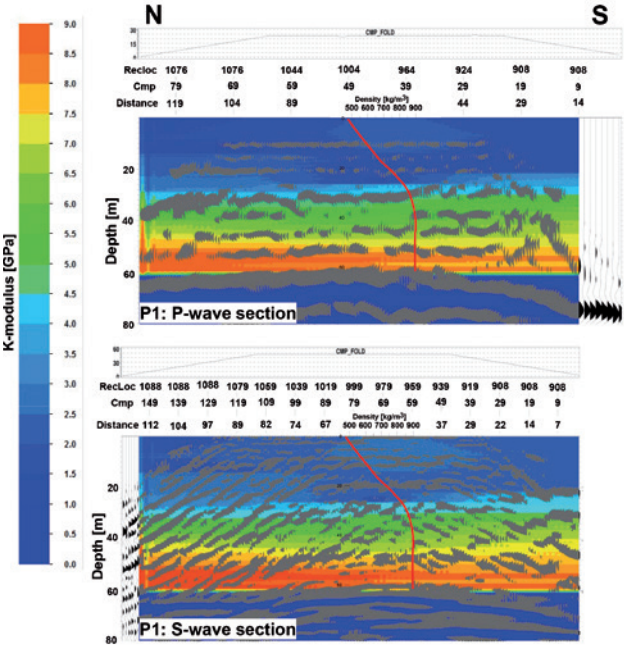

FIGURE 13

P- and S-wave depth sections (shaded) of profile 1 combined with a colour coded bulk modulus field in the background.

CONCLUSIONS

Shallow reflection seismic surveying at Colle Gnifetti demonstrated the principle capabilities of the vibroseis method for the investigation of firn and ice masses and underlying geological formations. The surprising results of the unique experiment also

show the capabilities of using a combined investigation of P- and S-waves with respect to the calculation of *in situ* elastic parameters of firn and ice formations and for the exploration of sub-ice geological structures. The resulting data quality was significantly better than shallow explosive charges used in an earlier experiment (Diez *et al.* 2013) and achieved more resolution and an increased productivity, even when a small vibroseismic source was used. The remaining depth uncertainty could not be clarified due to the lack of additional data for true depth calibration, which are required for further experiments.

ACKNOWLEDGEMENTS

We are grateful for the invaluable logistic support by the staff of Capanna Regina Margherita from the Club Alpino Italiano di Varallo/MBG Impresa and Hochalpine Forschungsstation Gornergrat. We would like to thank Air Zermatt for their flexibility in making the survey possible in the available short weather window. Many thanks also to Pascal Bohleber and Reinhard Drews for mutual assistance during field work. We also thank Günther Druivenga of GEOSYM for his enthusiastic support of the field work and for providing the ELVIS source for this experiment. Improvement of the manuscript was kindly supported by straight forward facts, English editing, comments and suggestions from Huw J. Horgan and Edward King, which are gratefully appreciated. Financial support for this study was provided to O.E. by the Deutsche Forschungsgemeinschaft (DFG) 'Emmy Noether' program Grant EI 672/6-1.

REFERENCES

Benjumea B. and Teixido T. 2001. Seismic reflection constraints on the dynamics of John Glacier, Antarctica. *Journal of Applied Geophysics* **46**(1), 31–44.

Bohleber P. 2008. *Age distribution and 18O variability in a low accumulation Alpine ice core: Perspective for paleoclimate studies*. Diploma Thesis, IUP Heidelberg.

Cuffey K.M. and Paterson W.S.B. 2010. *The Physics of Glaciers*, Fourth Edition. Elsevier textbooks, 704. ISBN-13: 9780080919126, ISBN-10: 008091912X

Diez A. 2013. Joint interpretation of explosive- and vibro-seismic surveys on cold firn for the investigation of ice properties. *Annals of Glaciology* **54**(64), 201–210.

Dix C.H. 1955. Seismic velocities from surface measurements. *Geophysics* **20**, 68–86.

Döscher A., Gäggeler H.W., Schotterer U. and Schwikowski M. 1995. A 130 years deposition record of sulfate, nitrate and chloride from a high-alpine glacier. *Water, Air and Soil Pollution* **85**(2), 603–609.

Dowdeswell J.A. and Evans S. 2004. Investigations of the form and flow of ice sheets and glaciers using radio-echo sounding. *Reports on Progress in Physics* **67**, 1821–1861.

Druivenga G., Grossmann E., Grüneberg S., Polom U. and Rode W. 2011. Transportabler Scherwellenvibrator. Deutsches Patent- und Markenamt, Patentschrift DE 103 27 757 A1. (in German)

Eisen O., Hamann I., Kipfstuhl S., Steinhage D. and Wilhelms F. 2007. Direct evidence for continuous radar reflector originating from changes in crystal-orientation fabric. *The Cryosphere* **1**, 1–10. http://www.the-cryosphere.net/1/1/2007/tc-1-1-2007.html

Eisen O., Hofstede C., Miller H., Kristoffersen Y., Blenkner R., Lambrecht A. and Mayer C. 2010. A new approach for exploring ice sheets and sub-ice geology. *Eos Transactions, American Geophysical Union* **91**(46), 429–430.

Eisen O., Nixdorf U., Keck L. and Wagenbach D. 2003. Alpine Ice Cores and Ground Penetrating Radar: Combined Investigations for Glaciological and Climatic Interpretations of a Cold Alpine Ice Body. *Tellus B* **5**(55), 1007–1017.

Etris E.L., Crabtree N.J. and Dewar J. 2001 True depth conversion*:* More than a pretty picture. *CSEG Recorder* **11**, 11–22.

Gammon P.H., Kiefte H., Clouter M.J. and Denner W.W. 1983. Elastic constants of artificial and natural ice samples by Brillouin spectroscopy. *Journal of Glaciology* **29**(103), 433–460.

Garotta R. 2000. Shear-waves from acquisition to interpretation. Distinguished Instructor Series 3, SEG, Tulsa.

Haeberli W. and Alean J. 1985. Temperature and accumulation of high altitude firn in the Alps. *Annals of Glaciology* **6**, 161–163.

Hofstede C., Eisen O., Diez A., Jansen D., Kristoffersen Y., Lambrecht A. and Mayer C. 2013. Investigating englacial reflections with vibro- and explosive-seismic surveys at Halvfarryggen ice dome, Antarctica. *Annals of Glaciology* **54**(64), 189–200.

King E.C. and Jarvis E.P. 2007. Use of shear waves to measure Poisson's ratio in polar firn. *Journal of Environmental and Engineering Geophysics* **12**(1), 15–21.

King E.C., Jarvis E.P. and Mowse E.A. 1993. Seismic characteristics of an airgun fired over snow. *Cold Regions Science and Technology* **21**(2), 201–207.

Kohnen H. and Bentley C.R. 1973. Seismoglaziologische Untersuchungen nahe Byrd Station, Antarktis. *Archives for Meteorology Geophysics and Bioclimatology Series A* **22**, 311–324.

Konrad H., Bohleber P., Wagenbach D., Vincent E. and Eisen O. 2013. Determining the age distribution of Colle Gnifetti, Monte Rosa, Swiss Alps, by combining ice cores, ground-penetrating radar and a simple flow model. *Journal of Glaciology* **59** (213), 179–189.

Moran M.L., Greenfield R.K.J., Arcone S.A. and Delaney A.J. 2000. Delineation of a complexly dipping temperate glacier bed using short-pulse radar arrays. *Journal of Glaciology* **46**(153), 274–286.

Polom U., Hansen L., Sauvin G., L'Heureux J.-S., Lecomte I., Krawczyk C.M. *et al*. 2010. High-resolution SH-wave seismic reflection for characterization of onshore ground conditions in the Trondheim harbor, central Norway. In: *Advances in Near-Surface Seismology and Ground-Penetrating Radar,* (eds R.D. Miller, J.D. Bradford and K. Holliger), pp. 75–92. SEG, Tulsa.

Pugin A.J.M., Larson T.H. and Sargent S.L. 2004. Near-surface mapping using SH-wave and P-wave seismic land-streamer data acquisition in Illinois, U.S. *The Leading Edge* **23**, 677–682.

Sen V., Stoffa P.L., Dalziel I.W.D., Blankenship D.D., Smith A.M. and Anandakrishnan S. 1998. Seismic Surveys in Central West Antarctica: Data and Processing Examples from the ANTALITH Field Tests (1994-1995), Antartica. *Terra Antarctica* **5**(4), 761–772.

Wagenbach D. (ed.) 2001. Environmental and Climatic Records from High Elevation Alpine Glaciers (ALPCLIM). Final EU-Project Report.

Yilmaz Ö. 2001. *Seismic Data Analysis*. Society of Exploration Geophysicists, Tulsa. Ziolkowski A.M. 1980. Wavelet deconvolution using a source scaling law. *Geophysical Prospecting* **28**, 872–901.

Ziolkowski A.M. 1980. Wavelet deconvolution using a source scaling law. *Geophysical Prospecting* **28**, 872–901.